

## Article

# The Role of Turbulent Coherent Structures on Microalgal Mixing for Nutrient Removal in Jet and Paddlewheel Raceway Ponds

Farhana Kayed <sup>1,\*</sup> , Sarik Salim <sup>2</sup>, Jennifer J. Verduin <sup>3,4</sup>  and Navid R. Moheimani <sup>3,5</sup><sup>1</sup> Department of Civil Engineering, Ahsanullah University of Science and Technology, Dhaka 1208, Bangladesh<sup>2</sup> School of Civil Environmental and Mining Engineering and UWA Oceans Institute, University of Western Australia, 35 Stirling Highway, Crawley, WA 6009, Australia<sup>3</sup> Environmental and Conservation Sciences, College of Science, Health, Engineering & Education, Murdoch University, Murdoch, WA 6150, Australia<sup>4</sup> Centre for Sustainable Aquatic Ecosystems, Murdoch University, Murdoch, WA 6150, Australia<sup>5</sup> Centre for Water, Energy and Waste, Harry Butler Institute, Murdoch University, Murdoch, WA 6150, Australia

\* Correspondence: farhanakayed@gmail.com

**Abstract:** Outdoor studies were conducted on microalgae cultures in two raceway ponds (kept in constant motion with either jet or paddlewheel) with a flatbed to treat anaerobic digestion piggery effluent and to observe the characteristics of turbulence on microalgal mixing and growth. Acoustic Doppler Velocimeters (ADV) were deployed to record the instantaneous velocity components and acoustic backscatter as a substitution of microalgae concentration. The present research on microalgal mixing considers the effect of event-based turbulent features such as the widely known ‘turbulent bursting’ phenomenon. This is an important aspect, as turbulent coherent structures can result in microalgal mixing, which can lead to significant changes in microalgal growth. The experimental results presented in this paper of two contrasting environments of jet- and paddlewheel-driven ponds suggested that: (1) turbulent bursting events significantly contributed to microalgal mixing when paddlewheels and jets were used; (2) among four type of turbulent bursting events, ejections and sweeps contributed more to the total microalgal mixing; and, (3) a correlation was revealed using wavelet transform between the momentum and microalgal mixing flux when either jet or paddlewheel were used. Such similarities in jet and paddlewheel raceway ponds highlight the need to introduce turbulent coherent structures as an essential parameter for microalgal mixing studies.

**Keywords:** anaerobic digestate of piggery effluent (ADPE); raceway ponds; flow rate; turbulent bursting; acoustic doppler velocimeter (ADV); microalgae mixing



**Citation:** Kayed, F.; Salim, S.; Verduin, J.J.; Moheimani, N.R. The Role of Turbulent Coherent Structures on Microalgal Mixing for Nutrient Removal in Jet and Paddlewheel Raceway Ponds. *Water* **2022**, *14*, 2824. <https://doi.org/10.3390/w14182824>

Academic Editors: Hongyu Ren and Fanying Kong

Received: 30 July 2022

Accepted: 5 September 2022

Published: 10 September 2022

**Publisher’s Note:** MDPI stays neutral with regard to jurisdictional claims in published maps and institutional affiliations.



**Copyright:** © 2022 by the authors. Licensee MDPI, Basel, Switzerland. This article is an open access article distributed under the terms and conditions of the Creative Commons Attribution (CC BY) license (<https://creativecommons.org/licenses/by/4.0/>).

## 1. Introduction

There is a worldwide interest in algal cultivation, especially to generate commodities [1] or high-value products [2], as well as to treat wastewater [3]. Raceway ponds are normally the most preferred microalgal cultivation system. Comprehensive knowledge of the physical processes that affect microalgal mixing has substantial implications for microalgal cells in their growth, as the high-magnitude turbulent flow can mechanically damage the cells, or otherwise interfere with growth processes [4,5]. This requires improved predictive turbulent models of microalgal mixing in raceway ponds. However, the mixing of microalgae is a complex mechanism from the micromechanics of fluid–solid interactions perspective, since describing turbulent flow’s fluctuating characteristic is difficult [6].

The fluid turbulent characteristics were conventionally only represented by a ratio known as the Reynolds number [4], widely used in characterizing fluid flow patterns. Further endeavors to characterize fluid flow suggest that it exclusively relies on fluid lifting force, with bottom boundary layer materials (considering microalgae as near-bed

material in our case) being uplifted due to instantaneous near-bed vertical velocity [7–10]. In comparison to such an understanding, Bagnold [11] postulated that when the small-scale fluid turbulent eddies dominate the vertical components of velocity by exceeding the material settling velocity, near-bed materials maintain suspension. This indicates that the flow must continuously entrain the near-bed materials at an equal rate of an upward terminal fall velocity to establish a dynamic equilibrium of near-bed material interchange [6]. Since earlier theoretical developments were inadequate to combine the turbulent coherent structures in near-bed material suspension and transport, additional endeavors leading further trials and analyzing the problem theoretically, founded on stochastic and deterministic methods, are required.

Kline et al. [12] recognized a periodic and episodic process in the bottom boundary layer, in which the lower boundary layer gradually expands and then agitates with the outer layer flow, commonly known as ‘turbulent bursting’ phenomenon. As detailed by Salim et al. [6], in this phenomenon, the low-velocity fluid streaks initially dislodge outward from the bed, causing a partial collapse, called ejection. Later, due to this violent collapse and disorderly upward expulsion, high-velocity fluid streaks rush towards the bed, which is named as sweep. With the chronological order of turbulent bursting involving ejections and sweeps [13], the turbulent coherent flow structures have been proven to play a vital role in bottom boundary layer material [14] resuspension and mixing processes.

The finding of the turbulent bursting phenomena prompted scientists to investigate the function of fluid turbulence in near-bed material mixing from the standpoint of particle instantaneous movements. As documented by Salim et al. [6], numerous laboratory studies have related turbulent boundary layer coherent structures to the resuspension or mixing of near-bed materials. Grass [15] determined that above a flatbed, ejection events are less likely to transmit momentum than sweep events. Falco [16] found in a lab experiment that a certain collection of turbulent coherent characteristics was critical for near-bed material movement. Additional investigations [17–20] have proven the importance of turbulent bursting events in near-bed material mixing in fluvial environments [17–20].

In recent times, Zhang et al. [21] attempted to identify the computable affiliation of the algal growth rate and the turbulent intensity in diverse turbulent circumstances. Their findings demonstrated that the growth rate of the *Microcystis-aeruginosa*-type microalgae increased in the turbulent environment compared to the still water environment. Based on the results of this study, an exponential function was suggested to be used to include the impact of flow turbulence in the current algal growth models, which, up until this point, had only taken into account the effects of nutrient supply, illumination, and temperature. Though many scholars have attempted to investigate the impact of small-scale turbulence on algal growth to unveil the natural phenomena through observations and tests, no relevant studies have been observed that considered the organic material mixing mechanism (microalgae in our case) in such detail towards the development of a precise ‘microalgae mixing model’ merging fluids’ turbulent bursting features.

Therefore, the overarching aim of this paper is to signify the importance of instantaneous events on microalgae mixing, which were not considered in the traditional raceway pond mixing approach that uses a time-averaged fluid velocity only to define the Reynolds number [22,23]. We aimed to simulate the hydrodynamic processes involved in two contrasting turbulent environments, i.e., jet and paddlewheel raceway ponds. The influence of hydrodynamics characterized by turbulent instantaneous features on the growth of microalgae was analyzed and proposed to incorporate the spatial–temporal probabilistic characteristics of turbulent bursting events in future microalgae mixing models. In this regard, we conducted outdoor growth experiments using raceway ponds under unidirectional conditions over a flatbed in order to record high-frequency acoustic data near the boundary layer. Multiple techniques were used to process the data after collection, such as Reynolds decomposition, quadrant analysis, and wavelet transformation, which clarified the turbulent features and their effect on microalgae mixing, both in jet and paddlewheel raceway ponds.

## 2. Materials and Methods

### 2.1. Microalgae Culture, Anaerobic Digestate of Piggery Effluent (ADPE), and Growth Media

The covered anaerobic digestion pond at the Medina Research Station in Kwinana, Western Australia provided the culture medium (ADPE) for this investigation (32°13'16" S, 115°48'30" E). Previously, Eltanahy et al. [22] conducted experiments in this undiluted ADPE facility to better comprehend the mixing rates for the optimal utilization of light and nutrients for increased biomass production and nutrient removal rates; however, the effects of turbulent coherent structures on the mixing process remained unexplored. Therefore, in this paper, we have further investigated the data discussed by Eltanahy et al. [22], and for this purpose, summarized the chemical composition of the ADPE in Table 1. A mixed population consortium of microalgae dominated by *Chlorella*, previously isolated and established from undiluted ADPE as detailed by Ayre et al. [24], was used in this work. To reach a predetermined cellular concentration, over the course of four months, microalgae were grown and maintained as batch cultures, with harvests and replacements occurring at regular intervals with fresh ADPE.

**Table 1.** Chemical composition of untreated and undiluted ADPE used for the growth of microalgae reproduced with permission from Eltanahy et al. [22].

Parameter	Value
Ammonia ( $\text{mg L}^{-1} \text{NH}_4^+\text{-N}$ )	960–1000
Total phosphate ( $\text{mgL}^{-1} \text{PO}_4\text{-P}$ )	25.0–26.5
Nitrite ( $\mu\text{g L}^{-1} \text{NO}_2\text{-N}$ )	8.0–8.5
Magnesium ( $\text{mg L}^{-1} \text{mg}$ )	165–175
Potassium ( $\text{mg L}^{-1} \text{K}$ )	530–545
Total iron ( $\text{mg L}^{-1} \text{Fe}$ )	8.5–9.5
Nitrate ( $\text{mg L}^{-1} \text{NO}_3\text{-N}$ )	14.0–14.5
Chemical oxygen demand, COD ( $\text{mg L}^{-1}$ )	1200–1350
Total nitrogen ( $\text{mg L}^{-1}$ )	1050–1101

### 2.2. Experimental Setup and Cultivation Conditions

Outdoor experiments in fiberglass race-way ponds were conducted at Murdoch University's Algae R&D Centre from 21 September 2015 to 11 January 2016 (Austral summer) [25]. Previously, using the same experimental facility, Indrayani [25] studied microalgae species and their potential to be cultured under outdoor conditions. In this paper, the first raceway pond, known as the paddlewheel pond (PWP), as detailed in Indrayani [25], was mixed using a standard four-blade paddlewheel, whereas in the second pond, a jet nozzle was used for mixing (Figure 1). The design of the jet nozzle was based on Parsheh et al. [26], and made from Polylactic Acid (PLA) using a 3D printer, and the pond was named as the Jet Nozzle Pond (JNP). An identical amount of microalgae stock culture was used to inoculate both raceway ponds. They were run at a fluid velocity of 0.30 m/s, which was measured using the tracer method using 1M HCl [27]. Freshwater was used to make up the amount of water lost to evaporation per day of the experiment prior to sampling. The Murdoch University Weather Station provided weather records showing solar irradiance and air temperature for the experiment's time frame (<http://www.met.murdoch.edu.au> first accessed on 21 September 2015). On alternate days, the ponds were sampled at 10 a.m. Cell counts, evaluations of photosynthesis, and measurements of the media's ammonium nitrogen concentration were all conducted using samples that were obtained. For further details of the sample collection process, please refer to Eltanahy et al. [22].

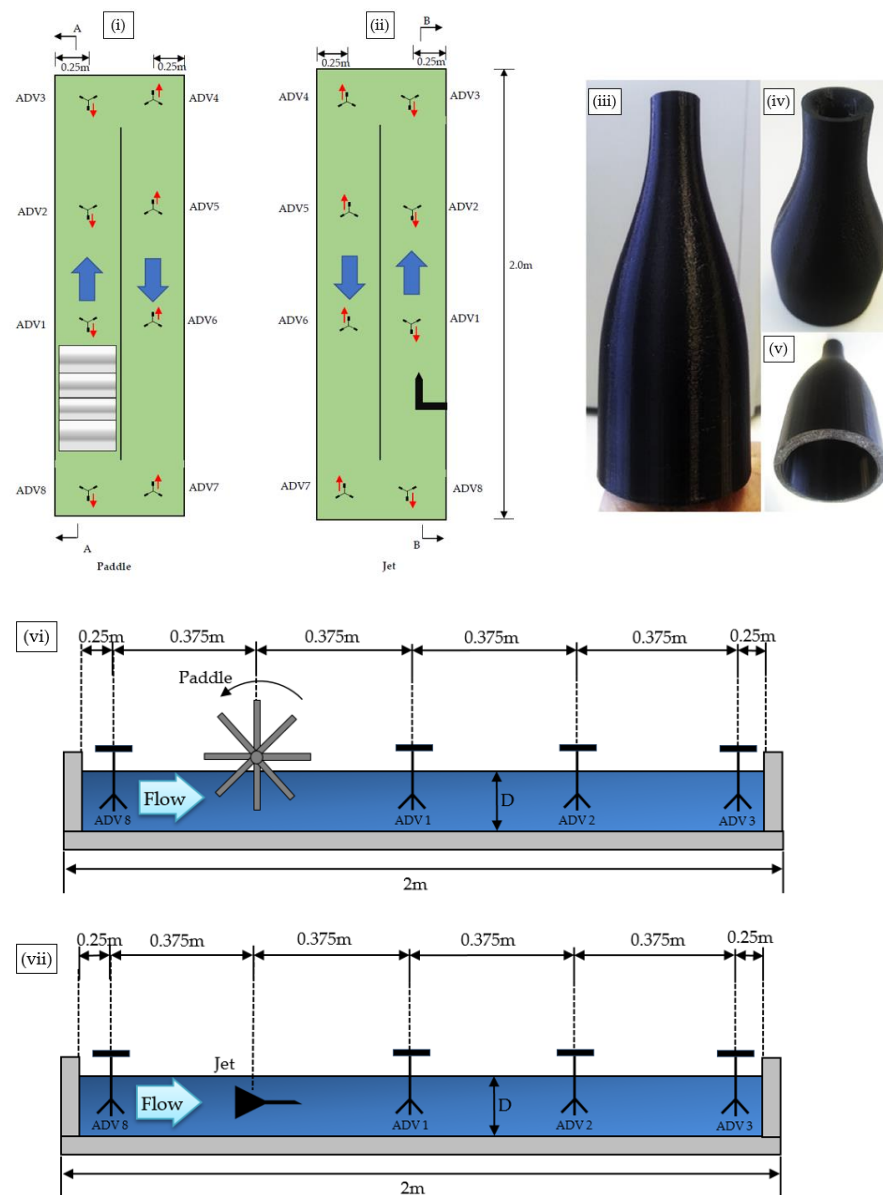


**Figure 1.** Experiment set-up of (i) PWP and (ii) JNP presenting the ADV measuring points in both the raceway ponds where red arrows indicate position of the ADV acoustic receiver (x), and (iii) side view of the nozzle, (iv) top view of the nozzle, (v) base view of the nozzle, (vi) section A-A of the experimental setup, (vii) section B-B of the experimental setup, reproduced with permission from Eltanahy et al. [22].

### 2.3. Data and Statistical Analysis

Though organic biomass (AFDW,  $\text{mgL}^{-1}$ ) was assessed in accordance with the procedures detailed by Moheimani et al. [1] by filtering 5 mL of culture through pre-combusted and pre-weighed GFC microfiber filters, the concentration of cell samples throughout time was evaluated using an upgraded Neubauer counting chamber. Filters were dried at  $90\text{ }^{\circ}\text{C}$  for 7 h to remove ash, and then they were burned at  $450\text{ }^{\circ}\text{C}$  for 6 h in a furnace. Using separate YSI 6-Series Multiparameter Sondes, the temperature, dissolved oxygen (DO), and pH of both ponds were observed in-situ. A photometer was used to measure the amount of ammonium (Spectroquant Move 100, kit models from Merck, Bayswater, VIC 3153, Australia).

Previously, Salim et al. [6] used Nortek Vectrino Acoustic Doppler Velocimetry (ADV) instruments to measure the three-dimensional instantaneous flow velocities to examine

the turbulent bursting effect on sediment particles. In this study, Micro-acoustic Doppler Velocimetry (MicorADV by SonTek, San Diego, CA, USA) was employed to determine the flow field's three velocity components in the PWP and JNP at eight points in each pond, as shown in Figure 1. The gadget uses a sample frequency of 10 Hz for 10 min at each location and is based on the Doppler effect's physical theory. In all the paddle and jet trials, as shown in Figure 1, the ADVs were positioned 0.07 m above the bed. Notably, the sensors were spaced high enough from the bed so that they did not contact the bottom of the flume during the ADV's data collection due to the physical dimensions of the devices [22]. For analysis purposes, near-bed ADVs data (at  $z = 0.07$  m height above the bed) are used in this study.

In order to analyze the three-dimensional inertial subrange spectrum, spectral energy cascade theory was used [28]:

$$E(k) = C_k \epsilon^{(2/3)} k^{(-5/3)}, \quad (1)$$

where  $E(k)$  is the wave-number-based energy spectrum;  $C_k$  is the experimentally determined Kolmogorov constant (which lies between 1.4–2.2 due to considerable uncertainty);  $\epsilon$  is the energy dissipation rate; and  $k$  is the wave number [29].

The turbulent properties were ascertained using Reynolds decomposition [29–31]:

$$u = \bar{u} + u', v = \bar{v} + v', w = \bar{w} + w', \quad (2)$$

where  $u$ ,  $v$ , and  $w$  represent the measured velocity components;  $u'$ ,  $v'$ , and  $w'$  represent the turbulent components;  $\bar{u}$ ,  $\bar{v}$  and  $\bar{w}$  are the mean velocity components. This breakdown permitted the measurement of the kinetic energy in relation to fluid turbulence.

The turbulent kinetic energy (TKE) at all sampling locations maintaining  $z = 0.07$  m height above the bed was also calculated using single-point measurements of turbulent velocity fluctuations (i.e.,  $u'$ ,  $v'$ , and  $w'$ ). Later, the TKE was used to calculate the near-bed shear stress:

$$\tau_{\text{TKE}} = 0.5\rho C_1 (u'^2 + v'^2 + w'^2), \quad (3)$$

where  $\tau_{\text{TKE}}$  represents the TKE shear stress,  $\rho$  represents the density of fluid, and  $C_1$  represents a coefficient, with a value ranging between 0.19 and 0.2 [32,33]. In order to estimate the TKE shear stress,  $C_1 = 0.19$  was used in this study.

The following equation was used to determine the TKE shear stress from the measurement of shear stress because the TKE-to-shear-stress ratio is constant [34]:

$$\tau_{\text{TKE}} = 0.19 \text{ TKE}, \quad (4)$$

This technique was earlier regarded as one of the reliable and dependable approaches for estimating near-bed shear stress in complicated flow fields [32,34]. The term  $u'w'$  represented TKE shear stress in this study due to the fact that no quantitative analysis of TKE shear stress was considered.

The values of Reynolds shear stress were calculated by:

$$\tau_{\text{Re}} = -\rho(u'w'), \quad (5)$$

where  $\tau_{\text{Re}}$  denotes the Reynolds shear stress, and  $\rho$  denotes the density of fluid. Similar to the TKE shear stress, the term  $u'w'$  represented turbulent Reynolds stress in this study.

Different turbulent occurrences were categorized using quadrant analysis, which also looked at their intermittent character and Reynolds stress contributions. In order to examine their significance, on a  $u'-w'$  plane, velocity deviations were plotted into quadrants [35,36]. With the use of this methodology, we were able to categorize the frequency of incidence of the respective event that takes place during the course of bursting as follows: ejection ( $u' < 0$ ,  $w' > 0$ ), sweep ( $u' > 0$ ,  $w' < 0$ ), up-acceleration ( $u' > 0$ ,  $w' > 0$ ), and down-deceleration ( $u' < 0$ ,  $w' < 0$ ) [6]. Due to the ease of its application, the popular 2D quadrant method (i.e.,

$u'-w'$  plane) was selected in this study's exploration of several elements of turbulent flow physics [6].

Continuous Wavelet Transform (CWT) was used to determine the temporal evolution of momentum and algal mixing flux of turbulent coherent formations close to the fluid boundary layer, as detailed in Grinsted et al. [37]. This allowed us to measure the contribution of coherent structures to the energy spectrum, and revealed their dynamics. Wavelet Coherence (WTC) was used to discover zones with strong shared influence and phase connections between the CWT of momentum and algae mixing flux. Since the wavelet was not entirely time-localized, a Cone of Influence (COI) was used to characterize the CWT and WTC power spectrum artefacts. Due to this, we avoided findings within the COI and visualized a lighter shadow in the power spectra. Grinsted et al. discussed the algorithm and theory in detail [37].

### 3. Results and Discussion

Three samples were used for the triplicate measurements of cell growth and ammonium concentration. The outcomes are presented as mathematical mean standard errors (SE), as shown in Table 2. The substantial dissimilarities between the different microalgae content parameters in the individual ponds were determined using a *t*-test. To compare significant differences between the various treatments and parameters, one-way repeated-measures (RM) one-way analysis of variance (ANOVA) was performed, followed by the post hoc test of Hol-Sidak. A *p*-value of 0.05 was used to determine significance. SigmaPlot Version 12.5 for Windows was used for all statistical analysis.

**Table 2.** Summary of growth conditions, ammonium removal rates, and cell density range of cultures when paddlewheel or jet used for mixing. Data are extracted from Eltanahy et al. [22].

Cultivation Period	21 August 2015–13 December 2015	
Solar irradiance range ( $W \cdot m^{-2}$ )	140–1112	
Air temperature range ( $^{\circ}C$ )	16–34	
Daily rainfall range (mm)	0–27	
Raceway pond type	Jet driven	Paddle wheel driven
Average ammonium removal rates (%) *	23.5 ± 4.42	36.8 ± 3.93
	Cell density range ( $\times 10^4$ )	
<i>Chlorella</i> sp.	280–420	5–650
Cyanobacteria	400–900	80–390

Note: \* Data are average  $\pm$  se,  $n = 5$ .

We randomly selected two time series from both JNP and PWP (i.e., ADV 6 data records from both experimental conditions) for further representation. Similar results were obtained from other data sets from all other ADVs that were used in this experiment.

Turbulent fluid flow has enormous eddies that shrink with time. In this progression, turbulent kinetic energy (TKE) is conveyed from large-scale to small-scale movements until fluid viscosity disperses into heat. In this energy sequence, the 'inertial subrange' falls between large sizes (i.e., turbulence creation zone) and smaller scales (i.e., turbulence dissipation zone). Due to the absence of local energy sources or sinks in the inertial subrange, the flux of energy from the wave numbers of high values must equalize with the dissipation rate. Therefore, digital Fourier transforms were used to conduct spectrum analysis, as well as turbulent energy related to the inertial subrange, i.e.,  $5/3$  slope, at all observed sites to confirm the existence of small eddy turbulence, as outlined by Eltanahy et al. [22]. Overall, the results suggested similarities in both the investigated time series shown in this study, i.e., ADV 6 for both JNP and PWP confirmed the presence of small

eddy turbulence that can excel the turbulent bursting phenomena. However, it is not common to detect the  $-5/3$  spectral slope in estimates close to the bed, since the slope of vertical velocity spectra in the subrange becomes far less steep the closer we move to the bed. Thus, the experimental spectral results stated by Eltanahy et al. [22] disclose the presence of turbulent eddies smaller in size for the mixing of several algal strains/species in the analyzed data.

The scatterplots of the Reynolds and TKE bottom shear stress for the JNP and PWP runs of the selected data sets are shown in Figure 2a,b. In the graphs of both JNP and PWP, higher bed shear stress terms (i.e., values were greater than  $0.5 \times 10^{-3} \text{ m}^2/\text{s}^2$  of TKE and Re shear stress term estimations of both JNP and PWP tests) were produced to generate microalgae mixing, which are verified with backscatter intensity in Figures 3b and 4b, respectively. Such disparity between TKE and Re shear stress approaches also showed the existence of coherent flow structures in fluid turbulence, causing extremely localized and persistent inconsistency close to the bed, disrupting the near-bed shear stress.

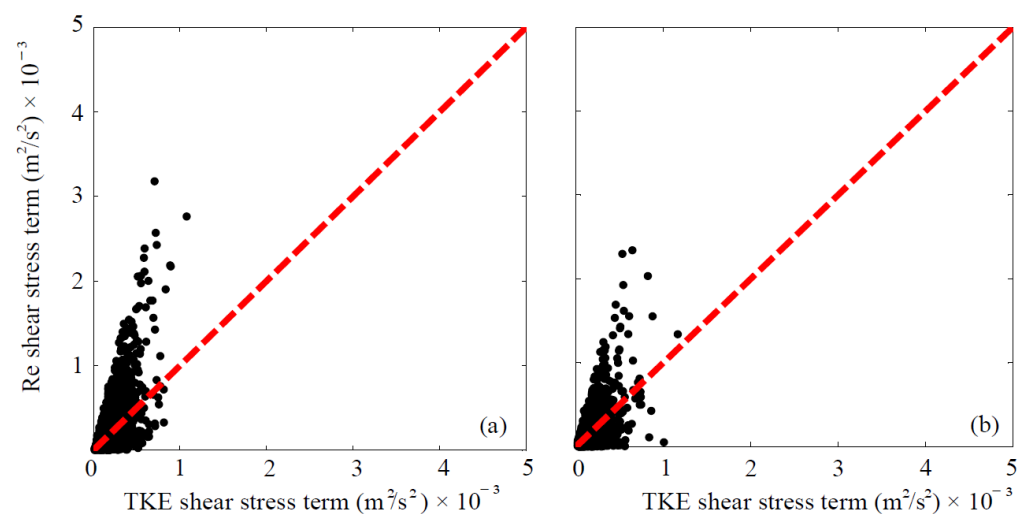


**Figure 2.** Contrast of the Reynolds and TKE shear stress term (one-second mean shown in black dots) from (a) JNP and (b) PWP experiments (for a twenty-five-minute period). The equality is defined by the dashed red line.

For both the JNP and PWP runs, we compared the identification of turbulent ejection and sweep events of the Reynolds shear stress ( $u'w'$ ) term and backscatter over a twenty-five-minute period (Figures 3 and 4, respectively). In both cases, we observed that the ejection and sweeps were the dominating events in the mixing of microalgae in the raceway ponds. This contrast offered a substantial perception of the involvement of turbulence relating to the events linked with microalgae mixing. Largely, substantial inconsistency and a sporadic pattern in both the Reynolds stress ( $u'w'$ ) term and microalgae mixing (backscatter) were also exposed in both of the time series. Previously, for other non-organic bed materials such as gravel and sand, this type of sporadic characteristic of  $u'w'$  been detected [6,15,19,31,38–44]. In more detail, forty-seven major algae mixing events were shown in the JNP time series (Figure 3). Twenty-seven of these events confirmed ejections, and twenty of these events revealed sweeps, which demonstrated that high-microalgae mixing events were more frequently linked with ejection and sweep turbulent motions than up-acceleration and down-deceleration motions during the examined periods (Table 3a). A similar arrangement was pragmatic for the twenty-five-minute PWP run, where forty-eight main mixing events were observed (Figure 4). Twenty-eight of these events were recognized as ejections, and twenty of these events were confirmed as sweeps (Table 3b). Such microalgae major mixing events of ejection and sweep identified in the JNP and PWP experiment show that turbulent bursting plays a vital role in microalgae mixing. In both tests, ejection and sweep events were the principal providers of momentum transfer. Up-

acceleration and down-deceleration events led to peripheral consequences on the transport of momentum and algae mixing flux in comparison to the other two events (Table 3). These findings suggest that vertical mixing, which is defined as the cyclical movement of algal cells between the surface and bottom layers of the culture, cannot be fully explained by relying just on the time-averaged Reynolds number. As a result, it is imperative that any future turbulent models for mixing algae take into account the spatial and temporal properties of turbulent flows, particularly the contribution of sweep and ejection events. Given the critical role that the vertical mixing of algae plays in preserving suspension and the light–dark cycle, special consideration should be given to include bursting phenomena as a crucial parameter in future models of the vertical mixing of algae. This will allow the best possible turbulent environment to be defined for the photosynthesis of algae.

**Table 3.** Major ejection (showed in bold letters) and sweep (showed in normal letters) events in the (a) JNP and (b) PWP experiments.

Test Run	Time (s)											
(a) JNP	47	62	<b>112</b>	130	<b>150</b>	202	<b>221</b>	276	<b>302</b>	<b>332</b>	<b>355</b>	<b>408</b>
	<b>444</b>	462	<b>510</b>	546	<b>564</b>	<b>582</b>	<b>628</b>	645	660	<b>675</b>	<b>710</b>	<b>752</b>
	766	<b>797</b>	836	<b>851</b>	900	<b>920</b>	945	<b>990</b>	<b>1022</b>	<b>1048</b>	1075	<b>1112</b>
	<b>1172</b>	1223	1263	<b>1300</b>	1320	1353	<b>1384</b>	<b>1414</b>	1437	1461	<b>1491</b>	-
(b) PWP	<b>33</b>	68	<b>88</b>	101	136	<b>186</b>	198	<b>216</b>	270	<b>312</b>	<b>354</b>	<b>384</b>
	<b>414</b>	462	<b>480</b>	<b>522</b>	546	<b>558</b>	<b>576</b>	<b>594</b>	642	660	<b>687</b>	<b>715</b>
	<b>749</b>	762	<b>789</b>	<b>809</b>	834	<b>846</b>	<b>852</b>	885	<b>911</b>	936	<b>972</b>	<b>1022</b>
	1064	<b>1110</b>	<b>1188</b>	1217	<b>1254</b>	1285	1325	<b>1332</b>	1362	<b>1398</b>	1440	1465

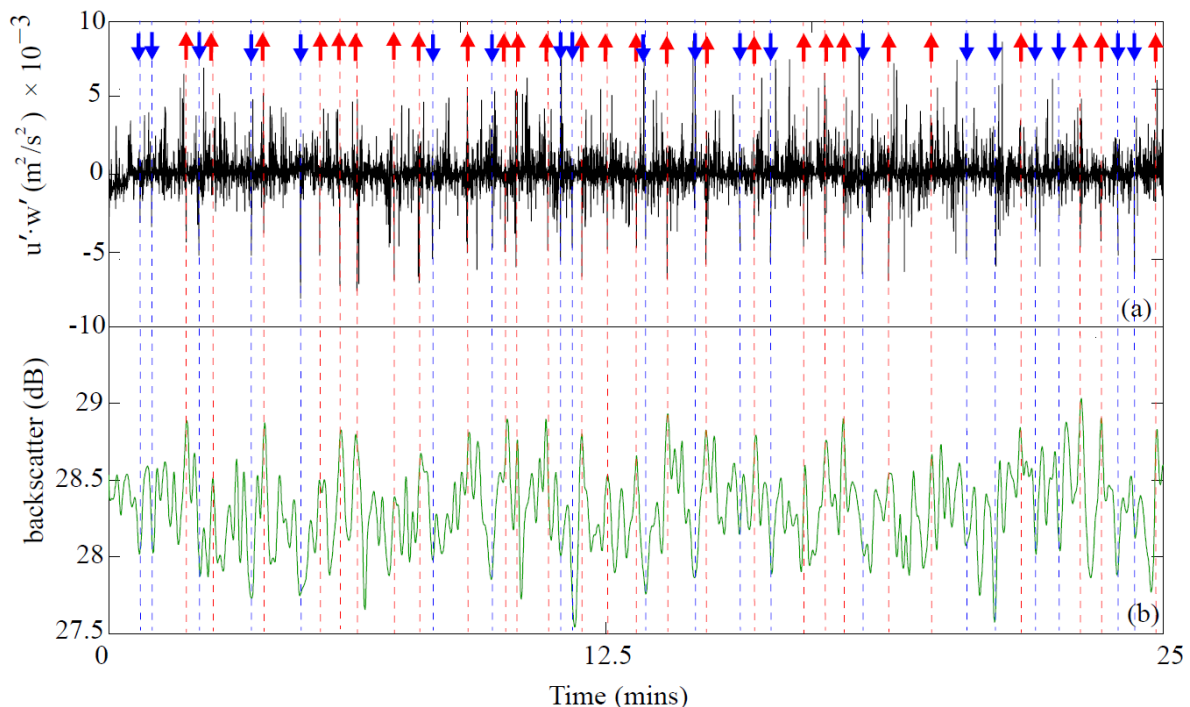


**Figure 3.** JNP experiment time series records: (a) turbulent Reynolds shear stress ( $u'w'$ ) term, ejection showed in red up-arrows and sweep showed in blue down-arrows; (b) backscatter (in one-second mean).

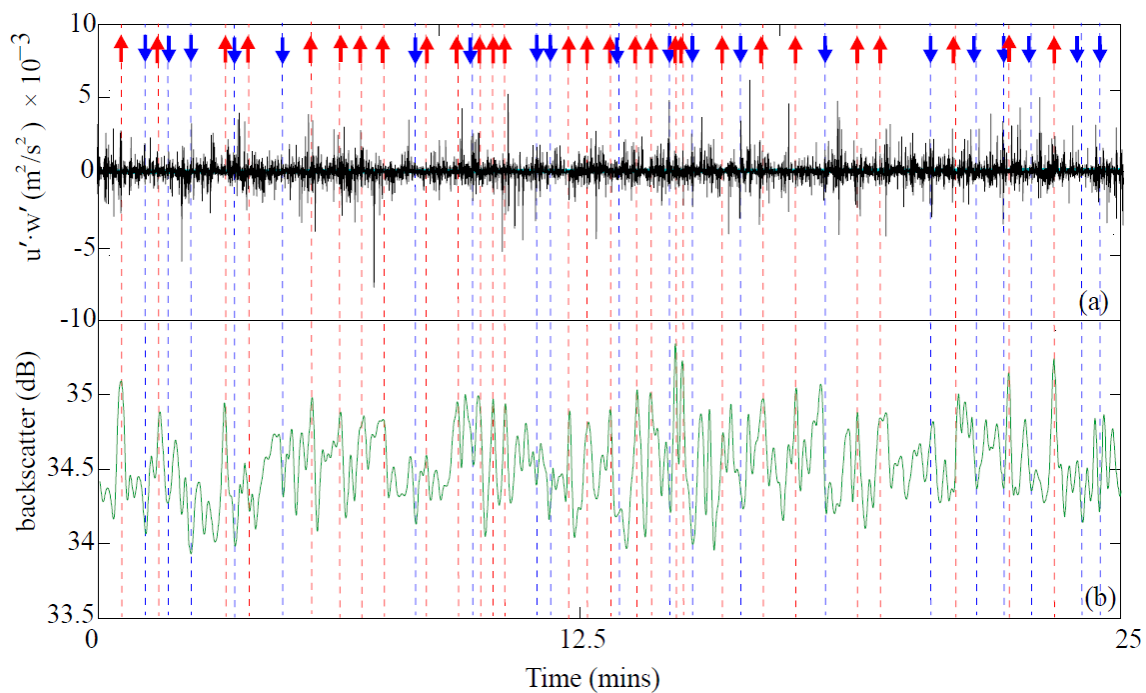


**Figure 4.** PWP experiment time series records: (a) turbulent Reynolds shear stress ( $u'w'$ ) term, ejection showed in red up-arrows and sweep showed in blue down-arrows; (b) backscatter (in one-second mean).

Contributions to  $u'w'$ , both for the JNP and PWP runs, were also detected in four quadrants of the  $u'-w'$  plane (Figure 5), where hole (H) = 1, 2, 3, 4 are small-to-medium events, and H = 5, 6, 7 are algae mixing events (i.e., backscatter reading above 10 dB). The graphs undoubtedly demonstrated that  $u'$  and  $w'$  contributed far more to ejections and sweeps than to up-acceleration and down-deceleration occurrences. The presented outcomes are comparable with preceding studies for the resuspension process of near-bed, non-organic materials [20,43]. Other data sets from both the JNP and PWP analyzed in this study also showed similar results.

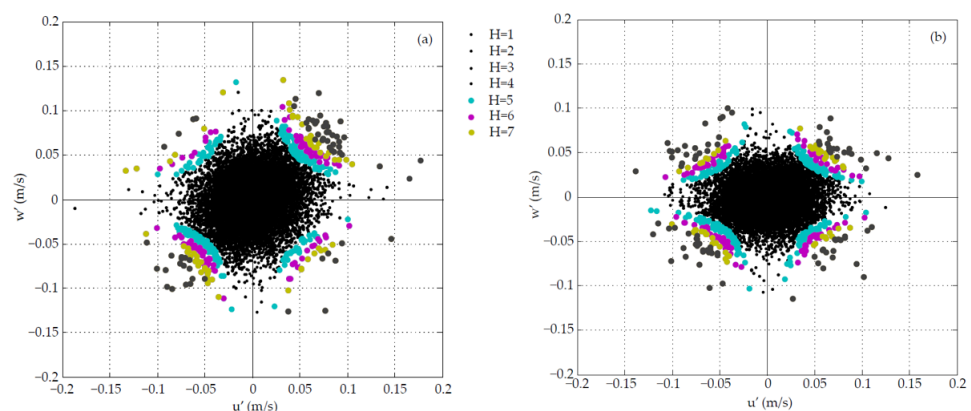


**Figure 5.** Turbulent bursting events in  $u'-w'$  space classification identifying ejection, sweep, up-acceleration, and down-deceleration events both for (a) JNP and (b) PWP experimental runs.

In order to define the occurrence of diverse turbulent bursting events and their significance to the Reynolds stress (i.e.,  $u'w'$ ), quadrant analysis was conducted. Table 4 shows the incidence proportions of four types of turbulent bursting motions, in addition to their contributions to the momentum ( $u'w'$ ) and microalgae mixing ( $c'w'$ ) fluxes for the JNP and PWP experiments. The observed outcomes for the  $u'w'$  indicators for the JNP and PWP

experimental runs agreed with the outcomes from previous investigations for non-organic bed materials [45,46]. For both JNP and PWP tests, ejection and sweep events were proven to be the leading source of the Reynolds stress; nevertheless, ejection contributed further to the net Reynolds stress, even though the time occupied by the ejection was less than that of the sweep (JNP = 47%; PWP = 45%), as shown in Table 4. Ejection (JNP = 42%; PWP = 44%) and sweep (JNP = 31%, PWP = 36%) mainly generated the upward algae mixing flux, and this indicated that the powerful upsurge of slow-moving fluid with high microalgae entrainment events was the prime basis of the total microalgae mixing flux. In comparison, up-acceleration (JNP = 14%; PWP = 10%) and down-deceleration (JNP = 13%; PWP = 10%) events carried less microalgae (Table 4). Thus, the total microalgae mixing flux was contributed to more by ejection and sweep events (JNP = 73%; PWP = 80%) than by up-acceleration and down-deceleration events (JNP = 27%; PWP = 20%). Such steady outcomes in both JNP and PWP endorse the need to investigate whether we should consider the instantaneous Reynolds stress concepts along the time-averaged microalgae mixing process in algae mixing models. Although the patterns of ejection and sweep contributions in the mixing process were very similar in the two very different environments of JNP and PWP, it is worth mentioning that high backscatter readings in JNP showed evidence of an improved mixing performance with higher shear stress on cultures in the JNP.

**Table 4.** Quadrant analysis of turbulent events.

	Time Occupied (in %)				Momentum Flux (in %)				Algae Mixing Flux (in %)			
	Ejection	Sweep	Up Acc	Down Dec	Ejection	Sweep	Up Acc	Down Dec	Ejection	Sweep	Up Acc	Down Dec
JNP	33	48	10	9	47	34	11	8	42	31	14	13
PWP	32	41	14	13	45	31	13	11	44	36	10	10

In both JNP and PWP runs, quadrant analysis revealed that ejection (where low-speed fluids travel away towards the outer layer from the boundary) entrained microalgae away from the flume bottom to maintain them in suspension. Sweeps (where high-speed fluid travels close to the flume bottom), with a negative influence, compressed the microalgae in resuspension by driving them near the bed of the flume. Furthermore, the time taken in both JNP and PWP runs to instantaneous momentum and algal mixing flux were almost similar and contributed identical percentages. Diplas et al. [47] experimented with non-organic sediment particles and established that the time-based length of such turbulent coherent impacts is also significant in defining the particle's entrainment of motion, and that their product, or impulse, is more suitable for postulating such circumstances in accumulation to the magnitude of the instantaneous turbulent forces applied on a particle. This was evident in both our JNP and PWP test runs, where, in contrast to the up-acceleration and down-deceleration events, the time taken by the ejection and sweep events (which were also demonstrated to play the leading role in the momentum and microalgal mixing fluxes) were considerably higher. Such insight of considering the time-based influence of bursting events discussed in this paper, as also argued by Diplas et al. [47] and Diplas and Dancey [48], demands attention to the hydrodynamic impulse (i.e., force multiplied by event time) as an inclusive condition in the improvement of future microalgae mixing models. We strongly recommend using the numerical parameter hydrodynamic impulse to evaluate the mixing using this statistical approach, which is based on the evaluation of the impact of turbulent bursting events on the algal cells. A computational fluid dynamic tool should be created to compute the vertical mixing mechanism of each cell.

Continuous Wavelet Transforms (CWT) and Wavelet Coherence (WTC) analysis [37] for JNP and PWP runs presented a more spontaneous method to picturize the turbulence data in both space and time (Figure 6). In the presented scalograms, the power experienced within the spectrum of COI (i.e., in the scalograms shown as the shaded region) at higher periods (i.e., low frequency events) restricted the ability to examine the time-based evolution

of the specific peak frequencies, as stated by Salim et al. [6]. Hence, the study was limited to inspect high-frequency events occurring at time scales up to 32 s for both runs. The dynamics of coherent structures and their estimated influence on the microalgal mixing flux were traced largely in the scalograms. It was also noticeable that inside the large-scale movements (presuming  $>0.5$  s bands as large-scale movements), there were multi-scale (e.g., in JNP time series between  $\sim 47$ – $62$  s, period band ranging  $\sim 2$ – $16$  s (large scale) and  $\sim 0.5$ – $2$  s (small scale); in PWP time series between  $\sim 789$ – $795$  s, period band ranging  $\sim 2$ – $16$  s (large scale) and  $\sim 0.5$ – $2$  s (small scale)) and a few fine-scale embedding (e.g., in JNP at  $\sim 752$ – $758$  s, period band ranging  $\sim 0.5$ – $2$  s; in PWP at  $\sim 644$ – $648$  s, period band ranging  $\sim 0.5$ – $2$  s) features. This suggested that near the bottom boundary layer, for both the JNP and PWP runs, the majority of the energy was condensed within the high period (warmer color  $>0.5$  s), related to the average flow properties for both fluxes (i.e., momentum flux and microalgal mixing flux). The highly energetic turbulent events (i.e., warmer color  $>0.5$  s) were observed to occur intermittently all over the time series (e.g., in JNP at 47, 62, 112, 130, 150, 202, etc.; in PWP, at 33, 68, 88, 101, etc.), particularly in progressively emerging clusters (considering clusters developed taking  $>3$  s time) that continued short periods (i.e., lasted  $<2$  s) in the leading streamwise-vertical plane of the flow near the bottom of the flume. At lower frequencies for both JNP and PWP runs, the larger clusters had a period band over  $\sim 1$  and 8 s, whereas the fast-evolving clusters before weakening (considering those lasting up to 2 s) stretched between a  $\sim 0.5$  and 2 s period band. This was seen in the color-coded contours (Figure 6) associated with ejection and sweep events for the JNP runs. For the PWP runs, similar results were evident for ejection and sweep events. Additionally, the momentum flux was linked to the contour in the microalgal mixing flux within similar period bands both in ejection and sweep events in the JNP runs, as shown in Figure 6. Identical patterns were also observed in the PWP runs, showing similar period bands in the ejection events; in the sweep events, the momentum and microalgal flux coincide with each other. For both runs, the WTC was applied to the momentum and microalgal mixing flux, where shared features were observed, as shown in Figure 6. During the identified ejection and sweep events, the coherence was noticeably higher (i.e., warmer color  $>0.5$  s) both for the JNP and PWP runs, signifying that the transport process critically depends on producing momentum flux by fluid turbulent structures to facilitate the algae mixing flux. This summarizes that for visualizing and detecting the coherent structures from the raw turbulent data, the cross-wavelet transform method was effective, which also empowered us to investigate the relationship between boundary layer turbulence structures and the microalgal mixing flux. These conclusions also limit the usefulness of the Reynolds number (constant along the pond sections) as a unique parameter to estimate the real level of vertical mixing in a raceway pond.

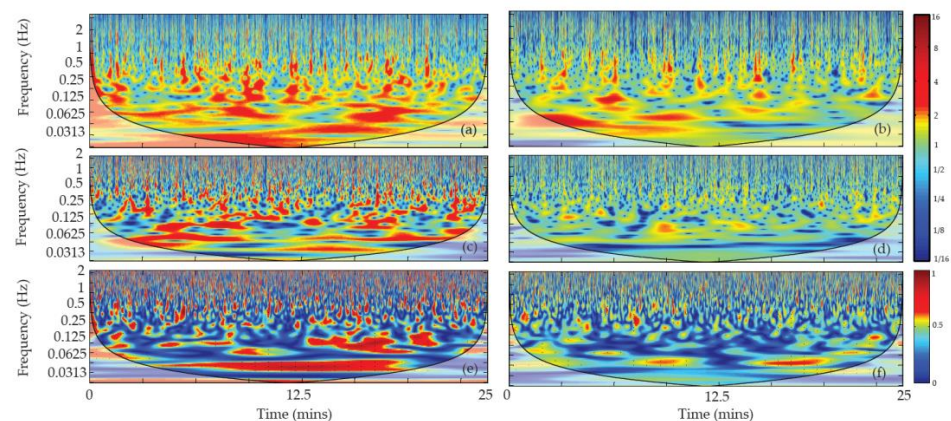


**Figure 6.** JNP and PWP experimental twenty-five-minute runs of wavelet power spectra (Morlet wavelet) showing the (a,b) momentum flux ( $u'w'$ ), (c,d) microalgae mixing flux ( $c'w'$ ), and (e,f) coherence between the momentum and algae mixing fluxes.

#### 4. Conclusions

Measurements were used in this study to examine the microalgal mixing processes due to turbulent coherent structures. To date, extensive investigation has been conducted to link turbulent coherent structures to describe the near-bed non-organic material resuspension process [21,23,49]; however, no one investigated the organic material mixing mechanism (microalgae in our case) in such detail towards the development of a precise 'microalgae mixing model' merging turbulence features. Two contrasting race ponds, one powered by a paddlewheel and the other by jet, were inspected in order to look at the mechanisms involved in the mixing process of microalgae, where it has been observed that turbulent bursting events have a significant contribution towards microalgal mixing. Particularly, in contrast to the up-acceleration and down-deceleration events, turbulent ejection and sweep events were more dominant to the total microalgal mixing. Ejection and sweep events were the major providers to the transfer of momentum in both the JNP and PWP test runs. Marginal effects were observed from the up-acceleration and down-deceleration events on the momentum transfer and algal mixing flux in comparison to the other two events. Wavelet analysis was beneficial to detect turbulence characteristics, which exposed a connection between the momentum and microalgal mixing flux when either jet or paddlewheel were used. Such similarities in the conditions of jet and paddlewheel raceway ponds highlight the need to introduce turbulent coherent structures as an essential parameter for microalgal mixing studies. Recent studies [21,23] incorporated fluid turbulence in their proposed mixing models, but the magnitude of turbulence was considered as time-averaged Reynolds stress. In order to boost pond productivity, the findings in this work open up new research directions that can provide thorough comprehensive knowledge of the interactions between fluid flow and algae mixing, as well as the rates of algal survival and growth under varied magnitudes of turbulence.

To improve the method on mixing evaluation based on a more in-depth statistical study of the various regions of the pond, further work is required to establish the ideal compromise between high vertical mixing and the optimal photosynthesis for modest energy inputs. Furthermore, more research needs to be conducted on the mechanical characteristics of the microalgae cell wall structure under the impact of turbulent mixing (including wall deformation and von Mises stress).

**Author Contributions:** F.K. analyzed, interpreted the data, and wrote the paper. S.S. conceptualized and designed the ADV data analysis and provided technical support. J.J.V. critically reviewed the article for important intellectual content and the final approval of the article, as well as provided administrative, technical, and logistic support. N.R.M. Conceptualized and designed the experimental works, provided critical revision of the article for important intellectual content, provided final approval of the article, and obtained the funding. All authors have read and agreed to the published version of the manuscript.

**Funding:** This research was partially funded by the Cooperative Research Centre for High Integrity Australian Pork (Pork CRC, Willaston, SA, Australia), grant number 4A-101112.

**Data Availability Statement:** The data that support the findings of this study are available upon request from the authors.

**Acknowledgments:** We are indebted to David Parlevliet for his work in printing 3-D nozzles. We would like to extend our thanks to Maryam Abdolohpour for her help with the use of ADV software, and the University of Western Australia for the loan of the micro ADVs.

**Conflicts of Interest:** The authors declare no conflict of interest.

#### References

1. Moheimani, N.R.; Webb, J.P.; Borowitzka, M.A. Bioremediation and Other Potential Applications of Coccolithophorid Algae: A Review. *Algal Res.* **2012**, *1*, 120–133. [[CrossRef](#)]
2. Ishika, T.; Bahri, P.A.; Laird, D.W.; Moheimani, N.R. The Effect of Gradual Increase in Salinity on the Biomass Productivity and Biochemical Composition of Several Marine, Halotolerant, and Halophilic Microalgae. *J. Appl. Phycol.* **2018**, *30*, 1453–1464. [[CrossRef](#)]

3. Raeisossadati, M.; Vadiveloo, A.; Bahri, P.A.; Parlevliet, D.; Moheimani, N.R. Treating Anaerobically Digested Piggery Effluent (ADPE) Using Microalgae in Thin Layer Reactor and Raceway Pond. *J. Appl. Phycol.* **2019**, *31*, 2311–2319. [[CrossRef](#)]
4. Moheimani, N.R.; Isdepsky, A.; Lisek, J.; Raes, E.; Borowitzka, M.A. Coccolithophorid Algae Culture in Closed Photobioreactors. *Biotechnol. Bioeng.* **2011**, *108*, 2078–2087. [[CrossRef](#)]
5. Nwoba, E.G.; Ayre, J.M.; Moheimani, N.R.; Ubi, B.E.; Ogbonna, J.C. Growth Comparison of Microalgae in Tubular Photobioreactor and Open Pond for Treating Anaerobic Digestion Piggery Effluent. *Algal Res.* **2016**, *17*, 268–276. [[CrossRef](#)]
6. Salim, S.; Pattiaratchi, C.; Tinoco, R.; Coco, G.; Hetzel, Y.; Wijeratne, S.; Jayaratne, R. The Influence of Turbulent Bursting on Sediment Resuspension under Unidirectional Currents. *Earth Surf. Dyn.* **2017**, *5*, 399–415. [[CrossRef](#)]
7. Einstein, H.A. *The Bed-Load Function for Sediment Transportation in Open Channel Flows*; Technical Bulletins No. 1026, September 1950; United States Department of Agriculture, Soil Conservation Service: Washington, DC, USA, 1950.
8. Velikanov, M.A. *Dynamics of Alluvial Streams*; State Publishing House for Theoretical and Technical Literature: Moscow, Russia, 1955; Volume 2.
9. Yalin, M.S. An Expression for Bed-Load Transportation. *J. Hydraul. Div.* **1963**, *89*, 221–250. [[CrossRef](#)]
10. Ling, C.-H. Criteria for Incipient Motion of Spherical Sediment Particles. *J. Hydraul. Eng.* **1995**, *121*, 472–478. [[CrossRef](#)]
11. Bagnold, R.A. The flow of cohesionless grains in fluids. *Philos. Trans. R. Soc. London. Ser. A Math. Phys. Sci.* **1956**, *249*, 235–297. Available online: <https://royalsocietypublishing.org/doi/10.1098/rsta.1956.0020> (accessed on 30 July 2022).
12. Kline, S.J.; Reynolds, W.C.; Schraub, F.A.; Runstadler, P.W. The Structure of Turbulent Boundary Layers. *J. Fluid Mech.* **1967**, *30*, 741–773. [[CrossRef](#)]
13. Robinson, S.K. Coherent Motions in the Turbulent Boundary Layer. *Annu. Rev. Fluid Mech.* **1991**, *23*, 601–639. [[CrossRef](#)]
14. Cao, Z.; Xi, H.; Zhang, X. Turbulent Bursting-Based Diffusion Model for Suspended Sediment in Open Channel Flows. *J. Hydraul. Res.* **1996**, *34*, 457–472. [[CrossRef](#)]
15. Grass, A.J. Transport of Fine Sand on a Flat Bed: Turbulence and Suspension Mechanics. In *Transport, Erosion and Deposition of Sediment in Turbulent Streams*; Institute of Hydrodynamic and Hydraulic Engineering, Technical University of Denmark: Lyngby, Denmark, 1974; Volume 48, pp. 33–34.
16. Falco, R.E. A Coherent Structure Model of the Turbulent Boundary Layer and Its Ability to Predict Reynolds Number Dependence. *Philos. Trans. R. Soc. Lond. Ser. Phys. Eng. Sci.* **1991**, *336*, 103–129. [[CrossRef](#)]
17. Kaftori, D.; Hetsroni, G.; Banerjee, S. Particle Behavior in the Turbulent Boundary Layer. I. Motion, Deposition, and Entrainment. *Phys. Fluids* **1995**, *7*, 1095–1106. [[CrossRef](#)]
18. Nelson, J.M.; Shreve, R.L.; McLean, S.R.; Drake, T.G. Role of Near-Bed Turbulence Structure in Bed Load Transport and Bed Form Mechanics. *Water Resour. Res.* **1995**, *31*, 2071–2086. [[CrossRef](#)]
19. Ninto, Y.; Garcia, M.H. Experiments on Particle—Turbulence Interactions in the near-Wall Region of an Open Channel Flow: Implications for Sediment Transport. *J. Fluid Mech.* **1996**, *326*, 285–319. [[CrossRef](#)]
20. Cellino, M.; Lemmin, U. Influence of Coherent Flow Structures on the Dynamics of Suspended Sediment Transport in Open-Channel Flow. *J. Hydraul. Eng.* **2004**, *130*, 1077–1088. [[CrossRef](#)]
21. Zhang, H.; Cui, Y.; Zhang, Y.; Xu, H.; Li, F. Experimental Study of the Quantitative Impact of Flow Turbulence on Algal Growth. *Water* **2021**, *13*, 659. [[CrossRef](#)]
22. Eltanahy, E.; Salim, S.; Vadiveloo, A.; Verduin, J.J.; Pais, B.; Moheimani, N.R. Comparison between Jet and Paddlewheel Mixing for the Cultivation of Microalgae in Anaerobic Digestate of Piggery Effluent (ADPE). *Algal Res.* **2018**, *35*, 274–282. [[CrossRef](#)]
23. Ali, H.; Cheema, T.; Park, C. Determination of the Structural Characteristics of Microalgal Cells Walls under the Influence of Turbulent Mixing Energy in Open Raceway Ponds. *Energies* **2018**, *11*, 388. [[CrossRef](#)]
24. Ayre, J.M.; Moheimani, N.R.; Borowitzka, M.A. Growth of Microalgae on Undiluted Anaerobic Digestate of Piggery Effluent with High Ammonium Concentrations. *Algal Res.* **2017**, *24*, 218–226. [[CrossRef](#)]
25. Indrayani, I. Isolation and Characterization of Microalgae with Commercial Potential. Ph.D. Thesis, Murdoch University, Murdoch, Australia, 2017.
26. Parsheh, M.; Smith, J.; Strutner, S.; Radaelli, G. Systems, Methods, and Media for Circulating Fluid in an Algae Cultivation Pond. US876 9867B2, 2014.
27. Raes, E.J.; Isdepsky, A.; Muylaert, K.; Borowitzka, M.A.; Moheimani, N.R. Comparison of Growth of *Tetraselmis* in a Tubular Photobioreactor (Biocoil) and a Raceway Pond. *J. Appl. Phycol.* **2014**, *26*, 247–255. [[CrossRef](#)]
28. Kolmogorov, A.N.; Levin, V.; Hunt, J.C.R.; Phillips, O.M.; Williams, D. The Local Structure of Turbulence in Incompressible Viscous Fluid for Very Large Reynolds Numbers. *Proc. R. Soc. Lond. Ser. Math. Phys. Sci.* **1991**, *434*, 9–13. [[CrossRef](#)]
29. Thomson, R.E.; Emery, W.J. Chapter 2-Data Processing and Presentation. In *Data Analysis Methods in Physical Oceanography*, 3rd ed.; Thomson, R.E., Emery, W.J., Eds.; Elsevier: Boston, MA, USA, 2014; pp. 187–218, ISBN 978-0-12-387782-6.
30. French, J.R.; Clifford, N.J. Characteristics and ‘Event-Structure’ of near-Bed Turbulence in a Macrotidal Saltmarsh Channel. *Estuar. Coast. Shelf Sci.* **1992**, *34*, 49–69. [[CrossRef](#)]
31. Kularatne, S.; Pattiaratchi, C. Turbulent Kinetic Energy and Sediment Resuspension Due to Wave Groups. *Cont. Shelf Res.* **2008**, *28*, 726–736. [[CrossRef](#)]
32. Biron, P.M.; Robson, C.; Lapointe, M.F.; Gaskin, S.J. Comparing Different Methods of Bed Shear Stress Estimates in Simple and Complex Flow Fields. *Earth Surf. Process. Landf.* **2004**, *29*, 1403–1415. [[CrossRef](#)]

33. Kim, S.-C.; Friedrichs, C.T.; Maa, J.P.-Y.; Wright, L.D. Estimating Bottom Stress in Tidal Boundary Layer from Acoustic Doppler Velocimeter Data. *J. Hydraul. Eng.* **2000**, *126*, 399–406. [[CrossRef](#)]
34. Pope, N.D.; Widdows, J.; Brinsley, M.D. Estimation of Bed Shear Stress Using the Turbulent Kinetic Energy Approach—A Comparison of Annular Flume and Field Data. *Cont. Shelf Res.* **2006**, *26*, 959–970. [[CrossRef](#)]
35. Lu, S.S.; Willmarth, W.W. Measurements of the Structure of the Reynolds Stress in a Turbulent Boundary Layer. *J. Fluid Mech.* **1973**, *60*, 481. [[CrossRef](#)]
36. Liu, D.; Liu, X.; Fu, X.; Wang, G. Quantification of the Bed Load Effects on Turbulent Open-Channel Flows. *J. Geophys. Res. Earth Surf.* **2016**, *121*, 767–789. [[CrossRef](#)]
37. Grinsted, A.; Moore, J.C.; Jevrejeva, S. Application of the Cross Wavelet Transform and Wavelet Coherence to Geophysical Time Series. *Nonlinear Process. Geophys.* **2004**, *11*, 561–566. [[CrossRef](#)]
38. Sumer, B.M.; Oguz, B. Particle Motions near the Bottom in Turbulent Flow in an Open Channel. *J. Fluid Mech.* **1978**, *86*, 109–127. [[CrossRef](#)]
39. Sumer, B.M.; Deigaard, R. Particle Motions near the Bottom in Turbulent Flow in an Open Channel. Part 2. *J. Fluid Mech.* **1981**, *109*, 311–337. [[CrossRef](#)]
40. Heathershaw, A.D.; Thorne, P.D. Sea-Bed Noises Reveal Role of Turbulent Bursting Phenomenon in Sediment Transport by Tidal Currents. *Nature* **1985**, *316*, 339–342. [[CrossRef](#)]
41. Drake, T.G.; Shreve, R.L.; Dietrich, W.E.; Whiting, P.J.; Leopold, L.B. Bedload Transport of Fine Gravel Observed by Motion-Picture Photography. *J. Fluid Mech.* **1988**, *192*, 193–217. [[CrossRef](#)]
42. NiNo, Y.; Lopez, F.; Garcia, M. Threshold for Particle Entrainment into Suspension. *Sedimentology* **2003**, *50*, 247–263. [[CrossRef](#)]
43. Yuan, Y.; Wei, H.; Zhao, L.; Cao, Y. Implications of Intermittent Turbulent Bursts for Sediment Resuspension in a Coastal Bottom Boundary Layer: A Field Study in the Western Yellow Sea, China. *Mar. Geol.* **2009**, *263*, 87–96. [[CrossRef](#)]
44. Schmeckle, M.W. The Role of Velocity, Pressure, and Bed Stress Fluctuations in Bed Load Transport over Bed Forms: Numerical Simulation Downstream of a Backward-Facing Step. *Earth Surf. Dyn.* **2015**, *3*, 105–112. [[CrossRef](#)]
45. Wallace, J.M.; Eckelmann, H.; Brodkey, R.S. The Wall Region in Turbulent Shear Flow. *J. Fluid Mech.* **1972**, *54*, 39–48. [[CrossRef](#)]
46. Willmarth, W.W.; Lu, S.S. Structure of the Reynolds Stress near the Wall. *J. Fluid Mech.* **1972**, *55*, 65–92. [[CrossRef](#)]
47. Diplas, P.; Dancy, C.L.; Celik, A.O.; Valyrakis, M.; Greer, K.; Akar, T. The Role of Impulse on the Initiation of Particle Movement Under Turbulent Flow Conditions. *Science* **2008**, *322*, 717–720. Available online: <https://www.science.org/doi/10.1126/science.1158954> (accessed on 30 July 2022). [[CrossRef](#)] [[PubMed](#)]
48. Diplas, P.; Dancy, C.L. Coherent Flow Structures, Initiation of Motion, Sediment Transport and Morphological Feedbacks in Rivers. In *Coherent Flow Structures at Earth's Surface*; John Wiley & Sons, Ltd: Oxford, UK, 2013; pp. 289–307, ISBN 978-1-118-52722-1.
49. Dey, S. Entrainment Threshold of Loose Boundary Streams. In *Experimental Methods in Hydraulic Research*; Geoplanet: Earth and Planetary Sciences; Rowinski, P., Ed.; Springer: Berlin/Heidelberg, 2011; Volume 1, pp. 29–48, ISBN 978-3-642-17474-2.